地 震 研 究 所 彙 報
Bull. Earthq. Res. Inst.
Univ. Tokyo
Vol. 78 (2003) pp. 67-74

Structure and Physical Properties of Fracture Zone Derived From Seismic Observations at the Nojima Fault and the Western Tottori Earthquake Fault, Japan

Keiichi Tadokoro*

Research Center for Seismology and Volcanology, Nagoya University

Abstract

Research on active faults, their structure, physical properties, and fault behavior during an earthquake cycle is important for the earthquake prediction. In this paper, we summarize the results of our seismological analyses of shear-wave splitting and injection-induced earthquakes on the basis of seismic observations at active faults. The shear-wave splitting observations performed on the fracture zone of the 2000 Western Tottori, Japan, earthquake revealed the fracture distribution inside the fracture zone, causing about 1% anisotropy. We can detect the detailed fracture distribution inside a fracture zone through shear-wave splitting observations with a dense (less than several kilometers in interval) seismic array set on and along the fracture zone. The analysis of earthquakes induced by water injection experiments at the Nojima fault, Japan, depicted that the fracture zone is permeable and has a low coefficient of friction immediately after the mainshock. Long-term monitoring of clustered microearthquake activity at the Nojima fault revealed the heterogeneity of crustal strength. We point out that we need to clearly define "fracture zone" for each research background in discussions of fracture zones because the thickness of the fracture zone varies depending on the research method.

Key words: fracture zone, physical property, fault behavior, shear-wave splitting, induced earthquak

1. Introduction

Research on active faults, as well as the physical basis of earthquake generation itself, is important for the earthquake prediction. Moreover, fault behavior during an earthquake cycle should be understood in detail. Sibson (1992) proposed a model of fault behavior called fault-valve action. The model predicts variations in the physical properties of a fault (for example, permeability and pore pressure) during an earthquake cycle. However, time scale and ranges of fluctuations of physical properties are not described in the model. Introducing a time axis and absolute values of parameters into such a fault behavior model would lead to an understanding of the complete fault behavior.

A fault is sometimes illustrated as a single plane. However, a fault has a fracture zone of a certain thickness (we mention the thickness of a fracture zone in Section 4). The structure and physical properties of a fracture zone are important factors to better understand the preparation and generation processes of a large earthquake. The physical properties of a fracture zone to be considered are, for example, seismic velocity, quality factor (Q-value), coefficient of friction, and permeability. We have been performing seismological observations at active faults, focusing on their structure and physical properties, for the last several years. In this paper, we summarize our seismological research at active faults and point out an ambiguity in an important

*e-mail: tad@seis.nagoya-u.ac.jp (Furo-cho, Chikusa, Nagoya, Aichi 464-8602, Japan)

parameter, which is fault thickness.

2. Fracture distribution in the fracture zone

Fault-parallel fractures generated by shear faulting during a mainshock are dominant inside the fracture zone of an earthquake fault. The physical properties of the fracture zone may be partly controlled by such fractures. It is, therefore, important to investigate the detailed fracture distribution inside the fracture zone to discuss the physical properties of a fault.

Fractures of shear fault origin can be detected by shear-wave splitting analyses of the fracture zone (Tadokoro *et al.*, 1999), which has been verified at the Nojima fault, Japan and the North Anatolian fault, Turkey (Tadokoro *et al.*, 1999; 2000; 2002 a). Shear-wave splitting is also a useful tool for monitoring the fault healing process (Tadokoro and Ando, 2002). In addition, shear-wave splitting observations with a seismic array on and along a fracture zone can be useful for detecting the detailed fracture distribution inside the fracture zone. To verify this, we carried out a temporary seismic observation in and around the aftershock region of the 2000 Western Tottori, Japan, earthquake (Tadokoro *et al.*, 2002 b). As a preliminary observation, we installed two seismic stations (SSB and UNO in Fig. 1) on the fracture zone. The result of the shear-wave splitting analysis at the two stations shows a bimodal distribution in the polarization direction of faster shear-waves with averages of N99–106°E and N149–151°E (Fig. 2 and Table 1). The former direction is parallel to the orientation of regional maximum horizontal compressional stress (σ_H) in the study area (e.g., Tsukahara and Kobayashi, 1991). This consistency shows that the anisotropy is caused by cracks of tectonic stress origin (stress-origin anisotropy), as proposed by Crampin (1978; 1987). The latter direction, on the other hand, obviously differs from the orientation of regional σ_H and is parallel to the strike of the aftershock alignment, i.e., the fault strike, of the 2000 Western Tottori earthquake. This coincidence suggests that the anisotropy has been caused by fault-parallel shear fractures generated by mainshock faulting (fault-origin anisotropy). We can infer the locations of fault-origin anisotropic regions by choosing the region where all of the ray paths of the earthquakes with the fault-origin anisotropy pass.

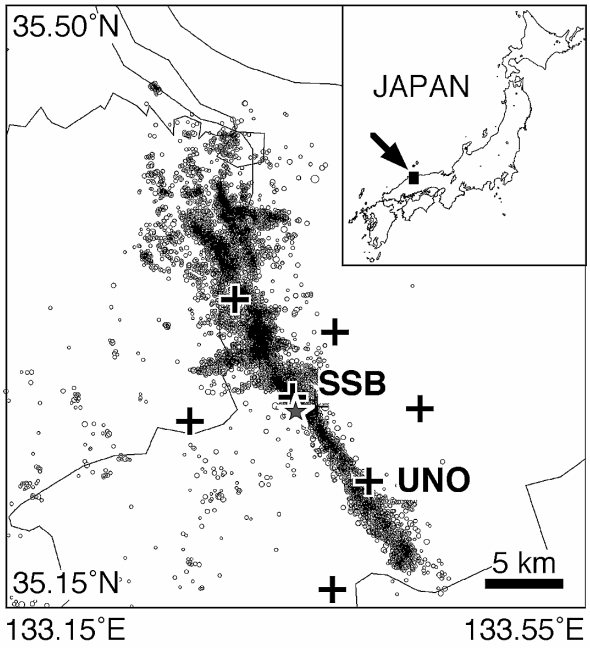

Fig. 1. Station distribution of our temporary seismic observations (crosses). Epicenters are plotted on the basis of the seismic catalog produced by Japan Meteorological Agency (JMA). The star denotes the epicenter of the 2000 Western Tottori earthquake determined by JMA.

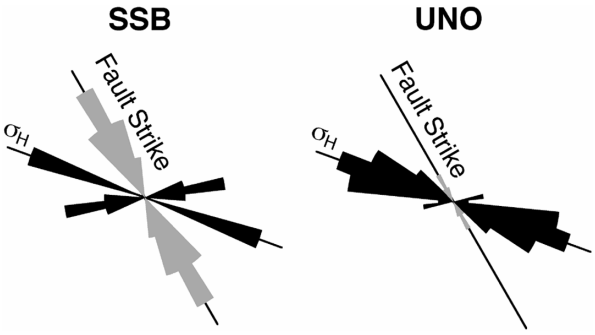

Fig. 2. Rose diagrams showing the polarization directions of faster shear-waves. The directions colored black and gray correspond to the polarization directions that are roughly parallel to the fault strike and to the orientation of regional maximum horizontal compressional stress (σ_H).

Table 1. Result of shear-wave splitting analysis.

SSB		UNO	
Direction[a], °	Delay Time[b], ms	Direction, °	Delay Time, ms
99±17	21±9	106±10	23±7
151±7	11±7	149±5	19±2

a: Polarization direction of faster shear-waves measured clockwise from north.

b: Time difference between faster and slower shear-waves.

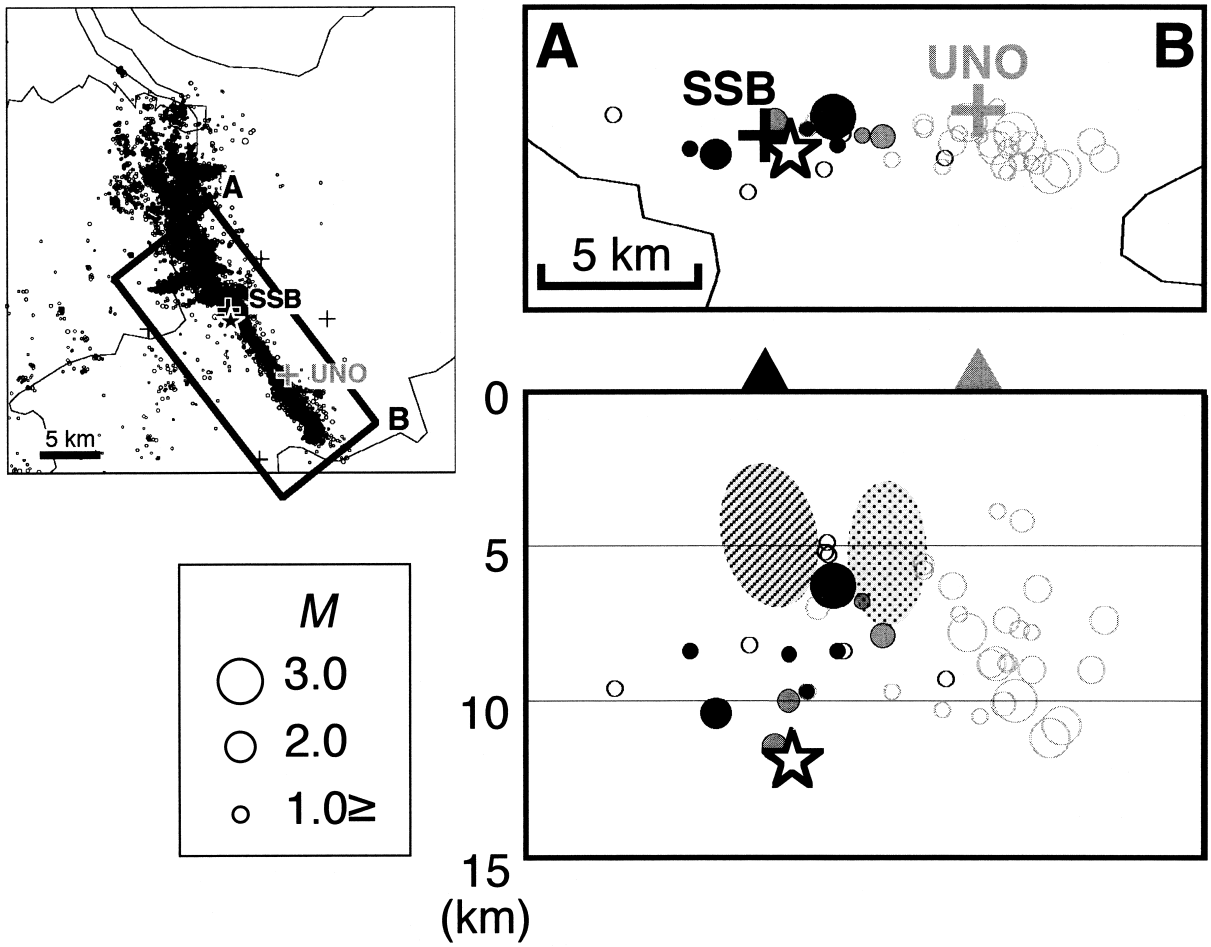

Fig. 3. Schematic illustration showing the locations of fault-origin anisotropic regions. The shaded and dotted portions are those estimated from analyses at SSB and UNO, respectively. Solid and open circles denote earthquakes showing fault-origin and stress-origin anisotropy, respectively. Earthquakes colored black and gray are used for the analyses at SSB and UNO, respectively. The star denotes the epicenter of the 2000 Western Tottori earthquake.

The inferred anisotropic regions are shown in Fig. 3. The fractures of shear fault origin are distributed in a particular region inside the fracture zone, and not throughout the fracture zone. Note that the reliability of the extent of anisotropic regions strongly depends on the density of seismic station and/or the hypocenters of earthquakes used for the analysis. In the case of the present observation, the distance between the two seismic stations on the fracture zone is about 7 km, and the extent of the anisotropic regions is unclear. Therefore, Fig. 3 gives the minimum extent of the anisotropic region. It is necessary to carry out observations with a denser seismic array with intervals of less than several kilometers to detect a more detailed fracture distribution.

Shear-wave splitting observations are suitable for deriving not only fracture orientations, but also the degree of fracturing quantified by the coefficient of anisotropy. Assuming a ray path propagating in the direction parallel to crack faces, the coefficient of anisotropy is approximately equivalent to $Vsdt/l$ (Leary *et al.*, 1990), where Vs is the shear-wave velocity without anisotropy, dt is time difference between the faster and slower shear-waves, l is the length of ray path in the anisotropic medium. The averages of dt for the earthquakes showing fault-origin anisotropy are 11 ms (SSB) and 19 ms (UNO), as listed in Table 1. On the basis of the illustration in Fig. 3, the value of l is inferred at about 5 km for all anisotropic regions. Substituting these values and $Vs=3.5$ km/s (Oike, 1975), the coefficients of anisotropy in the fault-origin anisotropic regions are estimated to be about 1%. Note that the estimated coefficient of anisotropy here is a rough estimate, because it strongly depends

Table 2. Outline of the water injection experiments.

	Date	Period, hrs	Total Amount of Water, m^3	Pumping Pressure, MPa	Flow Rate, 10^{-3} m^3/min
1997 1st	Feb. 9-13	74	49	2.8 - 4.3	8-10, 15
2nd	Mar. 16-25	216	209	4.0 - 4.7	16
2000 1st	Jan. 22-26	96	62.8	3.0	10-12
2nd	Jan. 31-Feb. 5	120	119.9	4.0	16-18
3rd	Mar. 3-11	192	273.0	4.5	20-26

on the length of the ray path in the anisotropic regions.

3. Fracture zone depicted by seismological research of the "Nojima Fault Zone Probe" project

3. 1. Physical properties of fracture zone derived from water injection experiments

Three boreholes with depths of 500, 800, and 1800 m were drilled at the Nojima fault after the 1995 Hyogo-ken Nanbu (Kobe), Japan, earthquake in the "Nojima Fault Zone Probe" project (Ando, 2001). Water injections were repeatedly performed as a part of the research subject of the Nojima Fault Zone Probe using the 1800-m-deep borehole in 1997 and 2000 (Shimazaki *et al.*, 1998; Nishigami, 2001). The purpose of the repeated water injection experiment is to monitor the fault-healing process and to detect fine structures of the fault zone. Each water injection is summarized in Table 2. The water was intermittently injected to the borehole twice and three times in 1997 and 2000, respectively. The total amounts of injected water in 1997 and 2000 were 258 m^3 and 456 m^3, respectively. In the 1997 experiment, we maintained a constant flow rate during each injection period. In the 2000 experiment, we controlled the flow rate to maintain constant values of pumping pressure.

We installed temporary seismic stations around the injection hole, including the 800-m-deep borehole seismometer, to monitor seismicity changes (induced earthquakes) accompanying the water injection experiments (Fig. 4). Fig. 5 shows cumulative curves for earthquakes with *S-P* times of less than 0.5 s at the 800-m-deep borehole station. In the 1997 experiment, obvious increases in seismicity ($-2<M<1$) were observed at 4–5 days after the beginning of each injection. We consider the increases in seismicity to have been induced by the injected water. The earthquakes occurred in the region about 3 km from the injection point and at 2 to 4 km in depth (Tadokoro *et al.*, 2000). We assume that the injected water has diffused inside the permeable fault zone. Under this assumption, the time interval between the beginning of injection and the timing of an abrupt increase in seismicity reflects the permeability of the fault zone. Solving a diffusion equation, the intrinsic permeability of the Nojima fault zone in 1997 is estimated to be $10^{-14}-10^{-13}$ m^2 (for details, see Tadokoro *et al.*, 2000). The values show that the Nojima fault in 1997 is more permeable than many other areas (Brace, 1984). In the 2000 experiment, while induced earthquakes were also observed at the same region as the 1997 experiment (Nagai *et al.*, 2001; Tadokoro *et al.*, 2001), the induced seismicity started 6–7 days after the beginning of each injection. The time interval is two days longer than that in 1997. The delay of two days implies a decrease in permeability in the fault zone due to fault healing. Adopting the same procedure as the 1997 experiment, the permeability in the Nojima fault zone is estimated to have decreased by 20–30% during the three years (Tadokoro *et al.*, 2001).

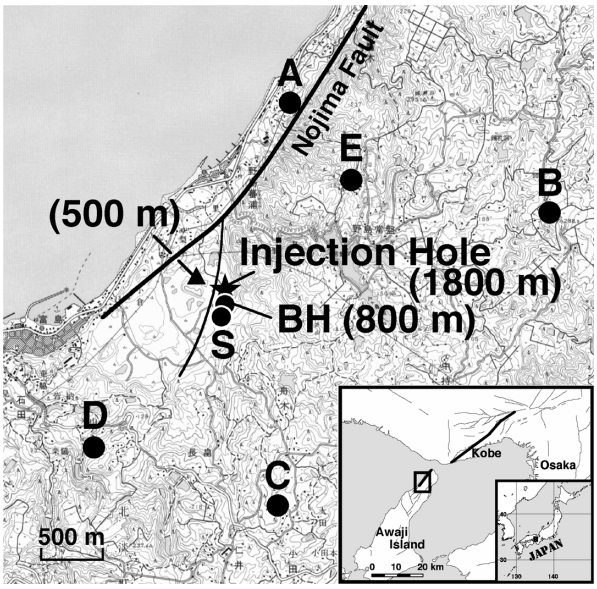

Fig. 4. Map showing surface positions of the boreholes (denoted as 500 m, 800 m, and 1800 m) and distribution of the temporary seismic stations (solid circles; A-E, S, and BH). BH denotes the 800-m-deep borehole. The star denotes the 1800-m-deep borehole used for the water injections.

A hydrofracturing test at a depth of 1.5 km in the 1800-m-deep borehole revealed that $\sigma_1 \approx \sigma_H = 45$ MPa and $\sigma_3 \approx \sigma_h = 32$ MPa (Tsukahara *et al.*, 2001), where σ_h is the minimum horizontal compressional stress. By

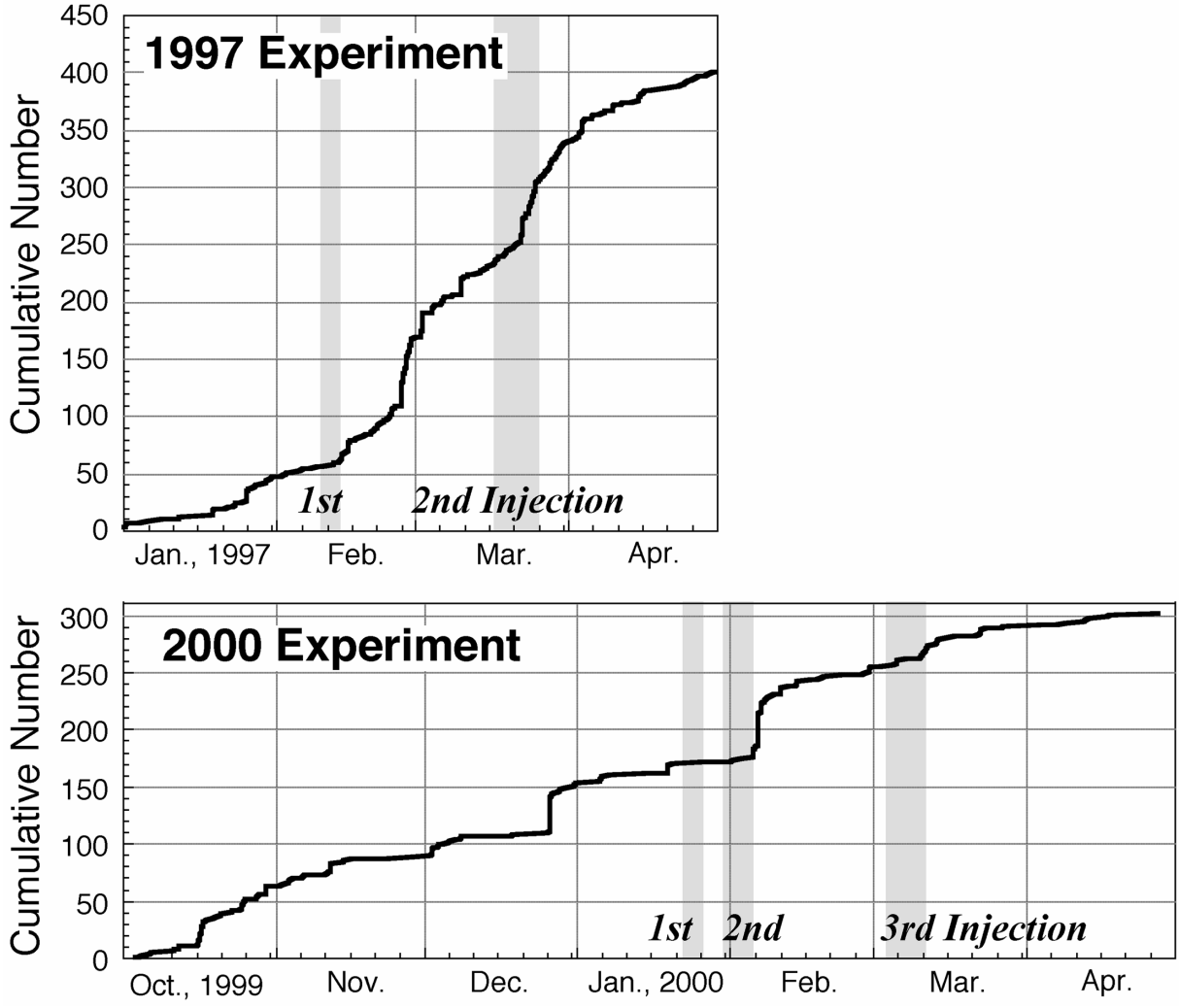

Fig. 5. Cumulative curve for earthquakes with *S-P* times less than 0.5 s at the 800-m-deep borehole seismometer. The periods of water injection are indicated by shading.

simply extrapolating these values (e.g., Zoback and Hickman, 1982; Iio, 1997), we estimate that $\sigma_1 \approx 88$ MPa and $\sigma_3 \approx 64$ MPa at 3 km in depth where the induced earthquakes occurred. Substituting these values into the equations representing the equilibrium of forces on a rupture plan and into the Coulomb criterion for shear failure, we obtained a coefficient of friction of less than 0.3 (for details, see Tadokoro *et al.,* 2000). The coefficient of friction obtained here is much smaller than those obtained from laboratory experiments ranging from 0.5 to 0.8 (e.g., Byerlee, 1978; Dieterich, 1981). A low coefficient of friction has also been suggested for the San Andreas fault (Zoback *et al.,* 1987; Byerlee, 1992).

3. 2. Heterogeneity of crustal strength derived from seismic activity

We observed not only the induced earthquakes but also many natural earthquakes with the temporary seismic network mentioned in the previous section. Some groups of microearthquakes show similar waveforms (Fig. 6). The waveform similarity suggests that their hypocenters are very close, that is, they form an earthquake cluster. The clustered seismic activities appeared among both the induced and natural earthquakes. Most of the earthquake clusters were formed within a few minutes to two hours. For example, 21 microearthquakes occurred in only two minutes in the earthquake cluster shown in Fig. 6.

A cross-spectrum analysis using the waveforms recorded at the 1800-m-deep borehole seismometer shows a result that the *S-P* time difference in each

cluster ranges from 3 to 20 ms (Tadokoro *et al.,* 2000; 2001). These values show that the regions of clustered seismic activity have sizes of 20–150 m or more. Fig. 7 shows the locations of earthquake clusters. The earthquake clusters are composed of the induced earthquakes concentrated in the same region as the natural earthquakes (denoted by the circle in Fig. 7). The coincidence in their occurrence region suggests that this region can rupture with an extremely small increase of shear stress or pore pressure. In other words, the strength in this region is relatively low in comparison to that of its surroundings. Taking account of successive ruptures of induced seismic activity in the region, the low strength may be caused by an extremely high crack density. The low strength region sometimes ruptures under the influence of localized stress concentration, then the clustered natural earthquakes occur. On the other hand, the pressured water injected during the present experiments selectively induces clustered seismic activity in this region.

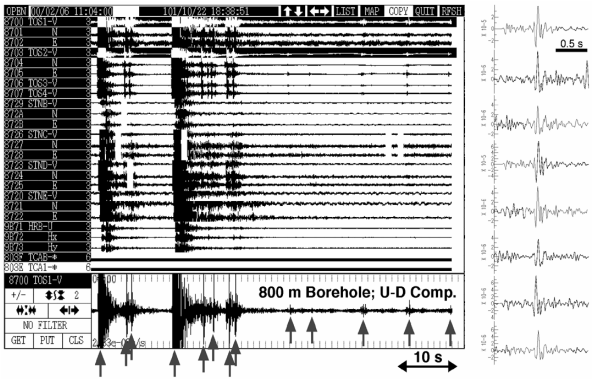

Fig. 6. Example of clustered seismic activity. (Left) Continuous seismograms for one minute from 11 : 04 : 00 (JST), February 6, 2000. Each earthquake is indicated by an arrow. (Right) Enlarged U-D component seismograms of eight earthquakes with relatively large amplitudes among 13 earthquakes in the left figure. All the earthquakes have similar waveforms.

4. Concluding remark

According to our research on the basis of the seismic observations, the following methods or observations are effective for deriving the structure and the physical properties of active faults:

(1) Shear-wave splitting observation on the fracture zone: Fracture distribution inside of fracture zone

(2) Water injection experiment: Physical properties of fracture zone (e.g., permeability, and coefficient of friction)

(3) Long-term monitoring of clustered microearthquake activity: Heterogeneity of crustal strength

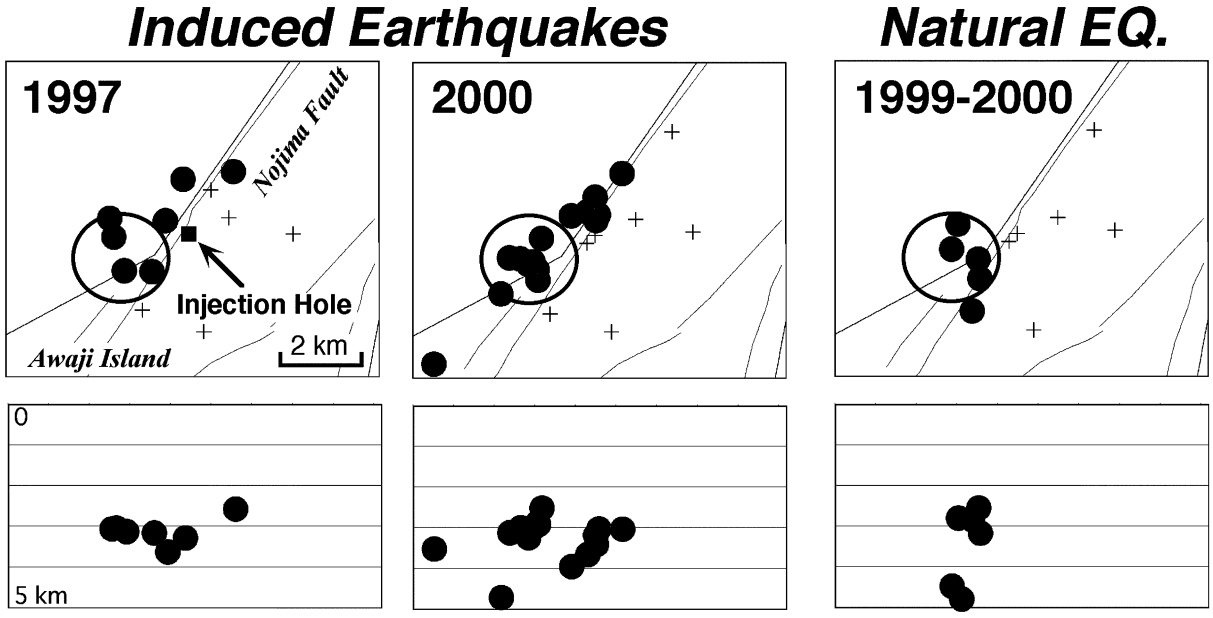

Fig. 7. Map views and cross-sections showing the locations of earthquake clusters. The hypocenters of largest earthquake in each cluster are plotted (solid circles). Earthquake clusters concentrated in the area denoted by large circles.

Observations of fault-zone trapped waves are also effective for deriving thickness of fracture zone, seismic velocity, and Q-value in fracture zones. Nevertheless, we omit the description on the fault-zone trapped wave in this paper because Mizuno (2003) summarized it.

The aspects of the fracture zone derived from our research are summarized as follows:

(1) Fault-parallel fractures generated by shear faulting during a mainshock prevail. The fractures cause ～1% anisotropy, in the case of the 2000 Western Tottori, Japan, earthquake.

(2) The above fractures are distributed in particular regions inside the fracture zone, and not throughout it. We can detect the fracture distribution inside a fracture zone by means of shear-wave splitting observations with a dense (less than several kilometers in interval) seismic array set on and along the fracture zone.

(3) The fracture zone is permeable and has a low coefficient of friction, less than 0.3, immediately after a large earthquake.

(4) The region of low strength, a weak region, exists around the Nojima fault. Clustered seismicity is repeatedly observed in the weak regions. The size of each cluster is 20–150 m or more. Most of the clustered earthquakes are small, and seismometers installed in boreholes are helpful to analyze them. This is because the seismometers on the Earth's surface supply seismograms with an extremely low signal-to-noise ratio.

For the purpose of understanding fault behavior during an earthquake cycle completely, it is necessary to monitor changes in the internal factors of a fault, such as permeability, coefficient of friction, and pore pressure, as well as external factors such as stress builed-up. A deep borehole drilled into the fracture zone might be the most appropriate tool to carry out monitoring.

A fracture zone is composed of central ultracataclasite layer, foliated zone, and damaged host rock, as classified in the structural model of Chester *et al.* (1993) (Fig. 8). We also need to solve an important problem: which portion in a fracture zone is effective in stress build-up, and preparation and generation processes for a large earthquake?

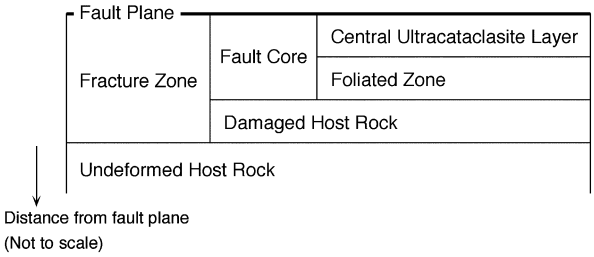

Fig. 8. Diagram summarizing a model of fault structure proposed by Chester *et al.* (1993).

The thickness of the fracture zone varies depending on the research method. For example, the thickness of the fracture zone of the Nojima fault, Japan, is estimated at 20–30 m from the fault-zone trapped waves (Ito and Kuwahara, 1995; Nishigami *et al.*, 1995; Li *et al.*, 1998), ～70 m (including the damaged host rock) from the boring cores (Tanaka *et al.*, 2001) and borehole results (Ito *et al.*, 1996), and several hundred meters from shear-wave splitting (Tadokoro *et al.*, 1999). Geochemical research is also able to characterize a fracture zone using differences in the chemical compositions of ground water. The research at the Atotsugawa fault, Japan, also revealed a thickness of the fracture zone more than several hundred meters, which is greater than that derived from a geological investigation (Satake and Murata, 1998). The groundwater, as well as the shear-wave splitting, is sensitive to the fractures, and the larger value for the fracture zone thickness is reasonable. Consequently, we need to clearly define fracture zone in each research in discussions of fracture zones, which will lead us to build a model of the fracture zone structure that is consistent with all geophysical, geological, and geochemical studies.

Acknowledgments

We would like to thank Drs. H. Ito and H. Mikada for their thoughtful reviews and many constructive comments. The temporary seismic observations at the Nojima fault were performed by the research group for Nojima fault water injection experiments, Nojima Fault Zone Probe. The research summarized in this paper was partly supported by Research Fellowship for young Scientists of Japan Society for the Promotion of Science (No. 13740267), and Grants-in-Aid of the Ministry of Education, Culture, Sports, Science and Technology, Japan (No. 10874063).

References

Ando, M., 2001, Geological and geophysical studies of the Nojima Fault from drilling: An outline of the Nojima Fault Zone Probe, *The Island Arc,* **10**, 206–214.

Brace, W.F., 1984, Permeability of crystalline rocks: New in situ measurements, *J. Geophys. Res.,* **89**, 4327–4330.

Byerlee, J.D., 1978, Friction of rocks, *Pure Appl. Geophys.,* **116**, 615–626.

Byerlee, J., 1992, The change in orientation of subsidiary shears near faults containing pore fluid under high pressure, *Tectonophysics,* **211**, 295–303.

Chester, F.M., J.P. Evans and R., L. Biegel, 1993, Internal structure and weakening mechanisms of the San Andreas Fault, *J. Geophys. Res.,* **98**, 771–786.

Crampin, S., 1978, Seismic wave propagation through a cracked solid: Polarization as a possible dilatancy diagnostic, *Geophys. J.R. Astron. Soc.,* **53**, 467–496.

Crampin, S., 1987, Geological and industrial implications of extensive-dilatancy anisotropy, *Nature,* **328**, 491–496.

Dieterich, J.H., 1981, Constructive properties of faults with simulated gouge, in *"Mechanical Behavior of Crustal Rocks: The Handin Volume, Geophys. Monogr. Ser.",* vol. 24, edited by N.L. Carter, M. Friedman, J.M. Logan, and D.W. Stearns, AGU, pp. 103–120.

Iio, Y., 1997, Frictional coefficient on faults in a seismogenic region inferred from earthquake mechanism solutions, *J. Geophys. Res.,* **102**, 5403–5412.

Ito, H. and Y. Kuwahara, 1995, Trapped waves along the Nojima Fault from the aftershock of Kobe earthquake, 1995, *Eos Trans. AGU,* **76**(46), 377, 1995.

Ito, H., Y. Kuwahara, T. Miyazaki, O. Nishizawa, T. Kiguchi, K. Fujimoto, T. Ohtani, H. Tanaka, T. Higuchi, S. Agar, A. Bri, and H. Yamamoto, 1996, Structure and physical properties of the Nojima fault by the active fault drilling. *Geophysical Exploration,* **49**, 522–35 (in Japanese).

Leary, P.C., S. Crampin and T.V. McEvilly, 1990, Seismic fracture anisotropy in the Earth's crust: an overview, *J. Geophys. Res.,* **95**, 11105–11114.

Li, Y.G., K. Aki, J.E. Vidale and M.G. Alvarez, 1998, A delineation of the Nojima Fault ruptured in the M7.2 Kobe, Japan, earthquake of 1995 using fault zone trapped waves, *J. Geophys. Res.,* **103**, 7247–7263.

Mizuno, T., 2003, The fault-zone trapped waves: the applications to investigation for the active faults in Japan, *Bull. Earthq. Res. Inst. Univ. Tokyo,* this issue.

Nagai, S., Y. Kano, K., Tadokoro, T. Mizuno, H. Yamanaka, S. Ohmi, K. Nishigami, Y. Hiramatsu and N. Hirata, 2001, Microseismic observations during a water injection experiment in 2000 at the Nojima fault, Japan, *Bull. Earthq. Res. Inst., Univ. Tokyo,* **76**, 163–186 (in Japanese).

Nishigami, K., 2001, Outline of water injection experiment, and shallow structure and healing process of the Nojima fault, *Chikyu Monthly,* **262**, 232–235 (in Japanese).

Nishigami K., Y. Fujiwara and Y. Shimada, 1995, Fault zone-trapped waves observed at the Nojima Fault for aftershocks accompanying the 1995 Kobe earthquake, *Eos Trans. AGU,* **76**(46), 378, 1995.

Oike, K., 1975, On a list of hypocenters compiled by the Tottori microearthquake observatory, *J. Seismol. Soc. Jpn.,* **28**, 331–346 (in Japanese).

Satake, H. and M. Murata, Water migration around the fault derived from ground water, *Chikyu Monthly,* **225**, 160–164 (in Japanese).

Shimazaki, K., M. Ando, K. Nishigami and N Oshiman, 1998, Water injection experiment at Nojima-Ogura, *Chikyu Monthly,* Extra **21**, 33–37 (in Japanese).

Sibson, R.H., 1992, Implications of fault-valve behavior for rupture nucleation and recurrence, *Tectonophysics,* **211**, 283–293.

Tadokoro, K., M. Ando and Y. Umeda, 1999, S wave splitting in the aftershock region of the 1995 Hyogo-ken Nanbu earthquake, *J. Geophys. Res.,* **104**, 981–992.

Tadokoro, K., M. Ando and K. Nishigami, 2000, Induced earthquakes accompanying the water injection experiment at the Nojima fault zone, Japan: Seismicity and its migration, *J. Geophys. Res.,* **105**, 6089–6104.

Tadokoro, K., Y. Kano, and K. Nishigami, 2001, Earthquake clusters accompanying water injection experiment, *Chikyu Monthly,* **262**, 264–267 (in Japanese).

Tadokoro, K. and M. Ando, 2002, Evidence for rapid fault healing derived from temporal changes in S wave splitting, *Geophys. Res. Lett.,* **29**, 10.1029/2001GL013644.

Tadokoro, K., M. Ando, S. Baris, K. Nishigami, M. Nakamura, S. B. U—er, A. Ito, Y. Honkura and A. M. Isikara, 2002 a, Monitoring of fault healing after the 1999 Kocaeli, Turkey, earthquake, *J. Seismology,* **6**, 411–417.

Tadokoro, K., A. Shimokawa, T. Mizuno and K. Nishigami, 2002 b, Asperity of the 2000 Western Tottori, Japan, earthquake fault derived from S-wave splitting analyses, *Eos Trans. AGU,* West. Pac. Geophys. Meet. Suppl., **83**(22), Abstract SE41B-08.

Tanaka, H., K. Fujimoto, T. Ohtani and H. Ito, 2001, Structural and chemical characterization of shear zones in the freshly activated Nojima Fault, Awaji Island, Southwest Japan, *J. Geophys. Res.,* **106**, 8789–8810.

Tsukahara, H. and Y. Kobayashi, 1991, Crustal stress in the central and western parts of Honshu, Japan, *J. Seismol. Soc. Jpn.,* **44**, 221–231 (in Japanese).

Tsukahara, H., R. Ikeda and K. Yamamoto, 2001, *In situ* strenn measurements in a borehole close to the Nojima Fault, *The Island Arc,* **10**, 261–265.

Zoback, M.D. and S. Hickman, 1982, In situ study of the physical mechanisms controlling induced seismicity at Monticello Reservoir, South Carolina, *J. Geophys. Res.,* **87**, 6959–6974.

Zoback, M.D., M.L. Zoback, V.S. Mount; J. Suppe, J.P. Eaton, J.H. Healy, D.H. Oppenheimer, P.A. Reasenberg, L.M. Jones, C.B. Raleigh, I.G. Wong, O. Scotti and C.M. Wentworth, 1987, New evidence on the state of stress of the San Andreas fault system, *Science,* **238**, 1105–1111.

(Received December 3, 2002)
(Accepted April 23, 2003)